

# RSC Advances



This is an *Accepted Manuscript*, which has been through the Royal Society of Chemistry peer review process and has been accepted for publication.

*Accepted Manuscripts* are published online shortly after acceptance, before technical editing, formatting and proof reading. Using this free service, authors can make their results available to the community, in citable form, before we publish the edited article. This *Accepted Manuscript* will be replaced by the edited, formatted and paginated article as soon as this is available.

You can find more information about *Accepted Manuscripts* in the [Information for Authors](#).

Please note that technical editing may introduce minor changes to the text and/or graphics, which may alter content. The journal's standard [Terms & Conditions](#) and the [Ethical guidelines](#) still apply. In no event shall the Royal Society of Chemistry be held responsible for any errors or omissions in this *Accepted Manuscript* or any consequences arising from the use of any information it contains.

# BiFeO<sub>3</sub> thin films on metallic Ni tapes by chemical solution deposition: effects of annealing temperature and a La<sub>0.5</sub>Sr<sub>0.5</sub>TiO<sub>3</sub> buffer layer on the dielectric, ferroelectric and leakage Properties

Xianwu Tang,<sup>a</sup> Ling Hu,<sup>a</sup> Jie Yang,<sup>a</sup> Li Chen,<sup>a</sup> Jianming Dai,<sup>a</sup> Wenhai Song,<sup>a</sup> Zhaorong Yang,<sup>a</sup> Xuebin Zhu,<sup>a\*</sup> and Yuping Sun,<sup>a,b\*</sup>

Received Xth XXXXXXXXXXXX 20XX, Accepted Xth XXXXXXXXXXXX 20XX

First published on the web Xth XXXXXXXXXXXX 200X

DOI: 10.1039/b000000x

In this article, BiFeO<sub>3</sub> (BFO) thin films are prepared on the metallic Ni (200) tapes with and without a La<sub>0.5</sub>Sr<sub>0.5</sub>TiO<sub>3</sub> (LSTO) buffer layer under different temperatures by chemical solution deposition. The effects of the annealing temperature as well as the LSTO buffer layer on the dielectric, leakage and ferroelectric properties have been studied in detailed. The crystallite size, dielectric constant and leakage current density increase, while the coercive field decreases with increasing annealing temperature. The BFO thin films deposited directly on the Ni tapes are prone to wrinkling, while the wrinkles are depressed via introducing a thin LSTO buffer layer. The decreased compressive microstrain as well as the improved ferroelectric and leakage properties is observed in the BFO thin films deposited on the LSTO buffered Ni tapes. The results will provide an instructive route to optimize BiFeO<sub>3</sub>-based thin films on the metallic tapes by chemical solution deposition methods.

## 1 Introduction

BiFeO<sub>3</sub> (BFO) thin films, over the last decade, have drawn significant interest and been widely investigated due to the ferro-

<sup>a</sup>Key Laboratory of Materials Physics, Institute of Solid State Physics, Chinese Academy of Sciences, Hefei 230031, China.

<sup>b</sup>High Magnetic Field Laboratory, Chinese Academy of Sciences, Hefei 230031, China.

\*Corresponding authors: [xbzhu@issp.ac.cn](mailto:xbzhu@issp.ac.cn) (Xuebin Zhu); [yypsun@issp.ac.cn](mailto:yypsun@issp.ac.cn) (Yuping Sun)

electric and magnetic properties at room temperature. BFO has a ferroelectric order with a Curie temperature of 850 °C<sup>1</sup>. One side, BFO thin films have complimentary ferroelectric polarizations as compared to the traditional ferroelectric lead zirconate titanate and the barium titanate thin films. These make the BFO interesting for usage in ferroelectric random access memories, optical modulators, waveguides, and micro-electromagnetic systems<sup>2</sup>. On the other hand, the characteristic of lead-free of BFO is promising for environment friendly devices. However, to date, the most of BFO thin films are deposited on the single-crystal substrates<sup>3,4</sup> and the platinized silicon wafers<sup>5-7</sup>. In an application point of view, such substrates are expensive cost, rigidity, and worthless in very limited sizes. Replacing these substrates by metallic tapes such as Ni, Cu, Al, and Fe is attractive commercially due to their low cost and simple pattern ability<sup>8</sup>. Additionally, among these base metals, Ni tape possessed lower resistivity, flexibility and other alluring functionality<sup>9</sup>. Technologically, integration of Ni tapes acted as inner electrodes and substrates within the capacitor into multilayer capacitors will be very important for device applications<sup>10</sup>. However, there are some problems of integrating an oxide ferroelectric thin film onto the metal tapes<sup>11,12</sup>. One problem is the possibility of substrate oxidation, which will depress the conductivity of the electrode. The other is the creation of a nonferroelectric interfacial layer caused by the interfacial reaction, and the interdiffusion between the substrate and the thin film, which will degrade the properties and the performances. Additionally, wrinkles resulted from the large misfits in thermal expansion coefficient and lattice constant between the ferroelectric thin film and the metal tapes will also downgrade the properties<sup>9</sup>. Nevertheless, these problems can be dissolved by induction of a buffer layer. As previous report<sup>13</sup>, a buffer layer is necessary to suppress the diffusion of metal atoms from the substrate to the thin film as well as the oxygen atoms from the thin film to the metal tape, and the wrinkles will be also depressed by the introduction of a buffer layer.

Recently, it is reported that the desired ferroelectric, piezoelectric, and magnetoelectric properties can be obtained in pulsed laser deposition (PLD)-derived BFO thin films directly on the Ni<sup>14</sup> and NiW<sup>15</sup> tapes. However, even though very high quality films can be made by PLD, the method is not very suitable for industrialization due to its expensive cost and the limited scale. Up to now, various methods have been used to prepare BFO thin films and to optimize their properties<sup>6,7,16-21</sup>. Among these methods, chemical solution deposition (CSD) is widely used due to its low cost, precise control of the stoichiometry, ability to achieve atomic-scale mixing, and easy processing of large-area thin films<sup>23</sup>.

In this article, BFO thin films are prepared on metallic Ni tapes by CSD. The effects of the annealing temperature as well as the introduction of a La<sub>0.5</sub>Sr<sub>0.5</sub>TiO<sub>3</sub> (LSTO) buffer layer

have been investigated systematically. The results will provide an instructive route to optimize BFO-based thin films metallic tapes by chemical solution deposition.

## 2 Experimental

Both the LSTO and BFO thin films were fabricated on the flexible Ni (200) tape via CSD methods. The LSTO buffered layers were deposited on the Ni tapes as our previous report<sup>24</sup>. The La-acetate, Sr-acetate, Ti-n-butoxide, and propionic acid were used as raw materials for preparing the LSTO precursor solution with a concentration of 0.1 M. Then, the thin films were prepared using a spin coater with a rotation speed of 4000 rpm with 30 s, pyrolyzed at 300 °C for 10 minutes in air, and then annealed at 900 °C in a forming gas (4% H<sub>2</sub>, and 96% N<sub>2</sub>) for 1 h. In order to enhance the thin film thickness, the spin coating, pyrolysis and annealing processes were repeated for two times, which gives the thin film thickness of about 20 nm.

BFO thin films were prepared by the CSD method as in our previous reports<sup>6,7</sup>. A 3 mol% excess amount of bismuth nitrate pentahydrate was used to compensate the bismuth loss during processing. BFO thin films were deposited on Ni (200) tapes with and without a LSTO buffer layer by spin coating. The thin films were annealed at different temperatures (475, 500, 525, and 550 °C) for 30 minutes in nitrogen atmosphere. Here, the BFO/Ni thin films annealed under 475, 500, 525, and 550 °C are denoted as N475, N500, N525 and N550 respectively, and the BFO/LSTO/Ni thin films annealed under 475, 500, 525, and 550 °C are denoted as NL475, NL500, NL525 and NL550 respectively.

The crystallization quality was checked via X-ray diffraction (XRD) using a Philips X'pert Pro diffractometer with a Cu K<sub>α</sub> radiation. Field-emission scanning electronic microscopy (FE-SEM, FEI Sirion 200 type, FEI, Hillsboro, OR) was used to detect both the thin film thickness and surface morphology, and all the thin films are with a thickness of about 488 nm. Top Au electrodes with 0.2 mm in diameter were deposited by sputtering by a small ion sputtering (SBC-12, KYKY, Beijing) onto the surface of BFO through a shadow mask. Dielectric response was investigated within the frequency range of 0-1 MHz with a driving voltage of 0.1 V by a precision inductance, capacitance, and resistance (LCR) meter (TH2828/A/S, Tonghui Electronic Co., LTD, Changzhou). The ferroelectric and leakage properties as well as the pulsed polarization positive up negative down (PUND) measurements at a pulse width of 0.05 ms and a delay time of 1s were investigated using a Sawyer-Tower circuit attached to a computer-controlled standardized ferroelectric test system (Radiant Precision Premier II, Radiant Technologies, USA).

## 3 Results and discussion

### 3.1 Microstructure

Figure 1(a) and (b) show the XRD patterns of the BFO/Ni and BFO/LSTO/Ni thin films, respectively. All the derived BFO thin films are randomly oriented without parasitic phases. Each diffraction peak of the BFO thin films can be indexed to a perovskite structure with a pseudocubic unit cell. The averaged crystallite size is calculated through the most three intense peaks naming of (001), (110) and (-110) peaks by the Scherrer equation. The variation of the derived crystallite size with the annealing temperature for the BFO/Ni and BFO/LSTO/Ni thin films is shown in the corresponding inset of Fig. 1(a) and 1(b), respectively. It is observed that the crystallite size increases lineally with increasing annealing temperature, no matter a LSTO buffer layer is used or not, which is same as the previous report<sup>7</sup>. Moreover, the BFO/LSTO/Ni thin films show the similar crystallite size as that of the BFO/Ni for each given annealing temperature. Both the results of the random orientation and the same crystallite size suggest that the LSTO buffer layer does not influence the nucleation in bulk of the BFO thin films.

Considering the existing misfit in thermal expansion coefficient and lattice constant between the BFO thin film and the metallic Ni tape, the strain induced by the substrate should be different in the BFO thin films under different annealing temperature. The residual strain in the films can be reflected directly by the change in lattice constant. Here, the lattice constant of the BFO thin films is calculated with the parameters of the three most intense diffraction peaks (001), (110) and (-110), based on the pseudocubic structure. The percentage change in lattice constant ( $\Delta a = (a - a_0)/a_0\%$  where  $a_0$  is take as 0.397 nm<sup>25</sup>) of each thin film is calculated and plotted in corresponding inset of Fig. 1. It can be seen that the percentage change in BFO lattice constant shows a negative value, and decreases slowly with increasing annealing temperature for both the BFO/Ni and BFO/LSTO/Ni thin films. The negative value indicates the compressive residual strain in the derived BFO thin films. The decreased negative value suggests that the compressive strain increases with the annealing temperature. As commonly observed in CSD-derived thin films, grain growth may be responsible for the microstrain partially relaxation<sup>7,26</sup>. While, here, the BFO thin films with large crystallite size display high residual strain. It implies that the residual strain in BFO/Ni thin films can not be relaxed via grain growth by increasing annealing temperature. On the other hand, the BFO/LSTO/Ni thin films exhibit a smaller value of strain, suggesting that the introduction of a LSTO buffer layer is beneficial for residual strain relaxation<sup>27</sup>. Considering the large thermal expansion coefficient misfit between the BFO and Ni tape, a high compressive stress will

be produced during the films cooling from the high annealing temperature. As a result, an increased compressive residual strain is displayed with increasing annealing temperature. Additionally, due to the small thermal expansion coefficient mismatch between the BFO and LSTO, a small microstrain will be produced in the BFO/LSTO/Ni thin films, although both the films exhibit a compressive residual microstrain in the same scale, as shown in insets of Fig. 1.

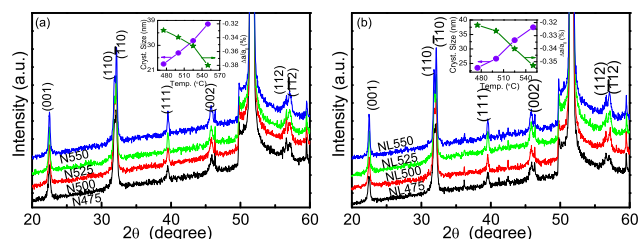


**Fig. 1** The XRD patterns of different temperatures annealed BFO thin films (a) BFO/Ni, and (b) BFO/LSTO/Ni. The variations of the averaged crystallite size and percentage change in lattice constant with the annealing temperature are shown in the corresponding inset.

Figure 2 shows the surface FE-SEM images of all derived BFO thin films. It can be observed that the BFO grain size increases with increasing annealing temperature for both BFO/Ni and BFO/LSTO/Ni thin films. Moreover, a different surface morphology between the BFO/Ni and BFO/LSTO/Ni thin films is exhibited as shown in Fig. 2, which can be attributed to the different grain growth due to the introduction of a LSTO buffer layer. Additionally, the BFO/Ni thin films are prone to wrinkling. As displayed in the insets of Fig. 2(a1)-(d1), the wrinkle edges indicated by the arrows in the reduced FE-SEM images are more visible. A clear interface layer without cracks is observed between the BFO layer, and Ni tape from the cross FE-SEM image, as shown in inset in the lower right corner of Fig. 2(d1). It is also observed two clear interface layers between the BFO, LSTO, and Ni tape, as displayed in inset of Fig. 2(d2), which indicates LSTO acting as an effective barrier to avoid possible atomic interdiffusion and reaction between BFO thin film and Ni tape. Additionally, the wrinkles increase and grow gradually with increasing annealing temperature. Usually, shrinkages due to densification will generate in the heating process in CSD-derived films<sup>28</sup>. At the same time, the hindrance of the viscous flow of the amorphous network associated with the substrate, strong tensile stresses parallel to the substrate will be induced, which can generate macroscopic heterogeneities such as macrocracks or wrinkles<sup>28</sup>. The appearance and increased wrinkles are preserved in the films during crystallized in high temperatures. On the other hand, the introduction of a LSTO layer will relieve the hindrance caused by the metallic Ni tape. As a result, the wrinkles are depressed in the BFO/LSTO/Ni thin films.

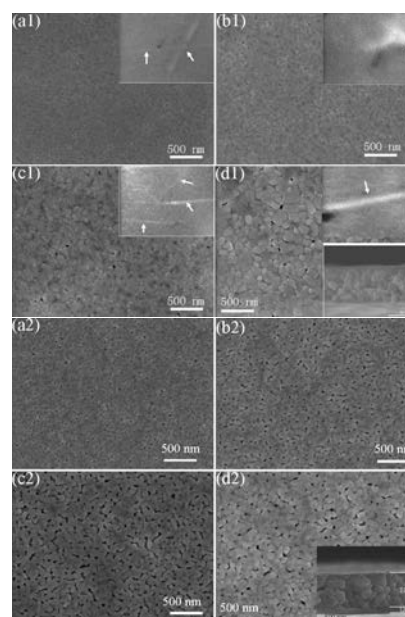


**Fig. 2** Surface FE-SEM images of the surface morphology of the BFO thin films (a) BFO/Ni, and (b) BFO/LSTO/Ni. The insets show the reduced FE-SEM results of the films BFO/Ni. Arrows indicate wrinkle edges. Insets in the lower right corner of (d1) and (d2) are the cross FE-SEM images of two typical films N550 and NL550, respectively.

### 3.2 Dielectric properties

The frequency dependent room temperature relative dielectric constant of all derived BFO thin films are shown in Fig. 3, and the dielectric loss of the corresponding films are displayed in the insets. The evolution of the dielectric constant measured at 1 MHz with the crystallite size is plotted in inset of Fig. 3(b). It is seen that within the measured frequency range the dielectric constant increases as well as decreases with increasing annealing temperature, which is same as our previous reports<sup>6,7</sup>. On the other hand, the dielectric constant almost increases linearly with increasing crystallite size as shown in the inset of Fig. 3(b). Moreover, for each given annealing temperature the BFO/LSTO/Ni thin films show a larger dielectric constant. It is well known that there are intrinsic and extrinsic contributions to the dielectric permittivity in the ferroelectric thin films<sup>29,30</sup>. The thin film orientation and crystallite size are the most important factors<sup>30</sup>. An increase in crystallite size will favor the formation of 180° domains, which can result in an enhanced dielectric constant<sup>30</sup>. Here, all the BFO thin films show subtle changes related to the orientation with increasing annealing temperatures. However, the increase in crystallite size with increasing annealing temperature as shown in Fig. 1 and 2, may favor the formation of the 180° domains, resulting in the enhancement of dielectric constant. Additionally, as

one of the extrinsic contributions to the dielectric permittivity, the grain boundary pinning and the mechanical strain/stress in the thin films can influence the dielectric response of the domain wall motion, and further affect the dielectric constant<sup>7,29</sup>. With increasing annealing temperature, the decreased pinning caused by the decreased in grain boundary will enhance the dielectric constant, although the increased microstrain as shown in Fig.1 will induce an inverse effect. For a given annealing temperature, the BFO/LSTO/Ni thin films have a lower microstrain, which will lead to a weak pinning resulting in a larger dielectric constant. On the other side, LSTO buffer layer may act as an effective barrier for the interfacial layer formation due to the atomic interdiffusion and reaction between the BFO thin film and the Ni tape during annealing process. Normally, the interfacial layer will result in the lowering of the dielectric constant due to the small permittivity of the interfacial layer<sup>6</sup>. Thus, the increase in dielectric constant with increased annealing temperature maybe originated from the increased crystallites size and the decreased grain boundary. The larger dielectric constant of the BFO/LSTO/Ni thin films is attributed to the decrease in pinning of domain wall motion induced by the enhanced strain relaxation as well as the reduction in interfacial effects. The decreased dielectric loss with decreased annealing temperature, and introducing a LSTO layer may be caused by the depressed electrical conduction (leakage current), as shown below.

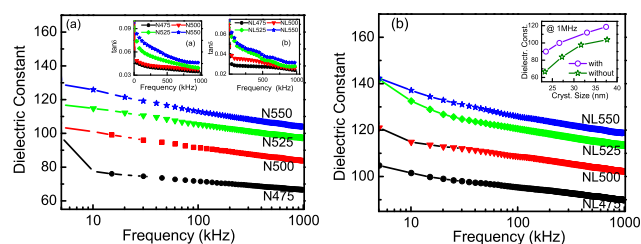


**Fig. 3** Log-scaled frequency dependent room temperature relative dielectric constant of the BFO thin films (a)BFO/Ni, and (b)BFO/LSTO/Ni. The corresponding dielectric loss is shown in the inset of (a). Inset of (b) shows the variation of the dielectric constant measured at 1 MHz with crystallite size.

### 3.3 Leakage properties

The leakage current density ( $J$ ) at room temperature in a log scale as a function of electric field ( $E$ ) for all derived BFO thin films is shown in Fig. 4. The  $J$  increases with increasing  $E$ , and the asymmetry can be attributed to the asymmetric electrodes<sup>6</sup>. The  $J$  value increases with increasing annealing temperature for both the BFO/Ni and the BFO/LSTO/Ni thin films. The increase in the  $J$  can be own to the increased oxygen vacancies due to the enhancement of crystallite size and

the decrease in grain boundaries as discussed in our previous reports<sup>6,7</sup>. On the contrary, for a given annealing temperature, the  $J$  of the BFO/LSTO/Ni thin films shows a much lower value compared with that of the BFO/Ni thin films. It implies that the usage of a LSTO buffer layer can improve the leakage properties in BFO thin films. The decrease in the leakage current density of the BFO/LSTO/Ni thin films is consistent with the fact that oxide electrodes can absorb oxygen vacancies<sup>31</sup>.

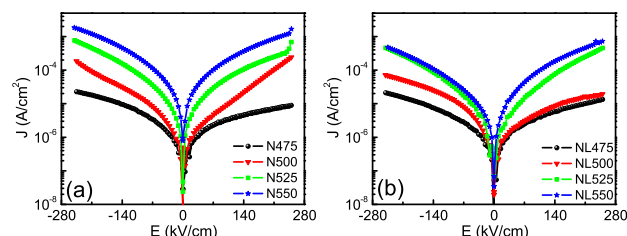


**Fig. 4** Room temperature leakage current density ( $J$ ) in log scale as a function of electric field ( $E$ ) for the derived BFO thin films (a)BFO/Ni, and (b)BFO/LSTO/Ni.

### 3.4 Ferroelectric properties

Figure 5 presents the evolution of the polarization with the applied electric field for all derived BFO thin films. In fact, the thin films annealed under low temperatures show good ferroelectric hysteresis loops regardless of the usage of the LSTO buffer layer. The higher the annealing temperature uses, the lower applied maximum electric field is needed to obtain a ferroelectric hysteresis loop. Although the BFO/LSTO/Ni thin films annealed at low temperatures exhibit low maximum polarization, they display much better ferroelectric hysteresis loops with sharp shape at the maximum electric fields. Additionally, as shown in Fig. 5, the coercive field ( $E_c$ , defined as the average electric field at the zero polarization) derived from the polarization-electric field hysteresis loops decreases with increasing annealing temperature. Moreover, the value of  $E_c$  for the BFO/LSTO/Ni thin films is smaller than that of the BFO/Ni thin films. The decrease in  $E_c$  with increasing annealing temperature can be attributed to two factors. One is the decrease in individual-domain grains induced by the enlarged grain size with increasing annealing temperature. The other one is the reduced clamping of domain walls due to the decrease in grain boundaries with increasing annealing temperature. As discussed above, the crystallite size of the derived BFO thin films is same when a LSTO buffer layer is used or not used. Thus, the contribution of the smaller  $E_c$  for the BFO/LSTO/Ni thin films is not originated from the variations of the individual-domain grains and clamping of domain walls. On the other side, as shown in the Fig. 2 and the inset of Fig. 1, the wrinkles are disappeared and the microstrain

is decreased for the BFO/LSTO/Ni thin films. Both two factors will depress the clamping of domain walls, resulting in the decreased  $E_c$ . On the other hand, as shown in Fig. 4, the decreased leakage current suggests the decrease in the charge carriers acted normally by the oxygen vacancy in the BFO thin films with a LSTO buffer layer. At the same time, the decrease in the oxygen vacancies can depress the pinning of the domain walls motion<sup>32</sup>, further leading to the lower  $E_c$  value. The reduced remnant polarization of the BFO/LSTO/Ni thin films should be caused by the same reasons. Additionally, the contribution of leakage current to the polarization cannot be avoided in measurements of ferroelectric hysteresis loops<sup>33</sup>, especially for the thin films with a high leakage. The improved leakage of the BFO/LSTO/Ni thin films will also give a contribution to the decrease in the remnant and maximum polarizations.

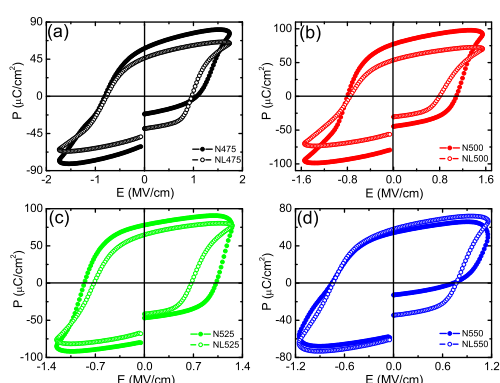


**Fig. 5** Evolution in the polarization with applied electric fields for the different temperatures (a) 475, (b) 500, (c) 525, and (d) 550 °C annealed BFO thin films BFO/Ni, and BFO/LSTO/Ni.

In order to eliminate the contribution of leakage current to the polarization as far as possible, a PUND measurement has been carried out with a varying field. The switched polarization value  $\Delta P$  derived from these measurements are shown in Fig. 6. For each given annealing temperature, the field dependent  $\Delta P$  of the derived BFO thin films is displayed in the insets of Fig. 6. The switched polarization values  $\Delta P$  derived from these measurements match well with the remnant polarization values obtained from the P-E loops. At a given applied electric field,  $\Delta P$  increases initially and then decreases with increasing annealing temperature. The increase in the  $\Delta P$  value is a result of two factors. One is the increase in multidomain grains as a consequence of grain growth with increasing annealing temperature. The other is the decreased pinning of the domain wall caused by the reduced grain boundary. However,  $\Delta P$  of the thin films N550 and NL550 displays a lower value, which should have a larger one due to the larger crystallite size and less grain boundaries. Combining the microstrain and wrinkles results, the decreased  $\Delta P$  can be attributed to the

enhanced pinning or constraining of the polarization domain wall motion caused by the increased compressive microstrain with increasing annealing temperature. Similarly, for each given annealing temperature, the depressed wrinkles and the low compressive microstrain<sup>32</sup> may be the one reason caused the large switched polarization of the derived BFO/LSTO/Ni thin films. On the other hand, the decreased oxygen vacancies as discussed above may be another reason, resulting in the decreased clamping on the domain walls<sup>34</sup>. As a result, less numbers of domains are pinned, and a larger switching polarization value is exhibited. Generally, the variation of ferroelectric properties with annealing temperature is the results of the increased crystallite size and the microstrain, as well as the decreased grain boundaries. The crystallite size may be a major factor of affecting the ferroelectric properties of the BFO/Ni thin films. For these thin films with same crystallite size, the ferroelectric properties are affected by the thin film strain. The improved ferroelectric properties of the BFO/LSTO/Ni thin films are mainly caused by the depressed wrinkles and the reduced microstrain as well as the improved leakage properties.

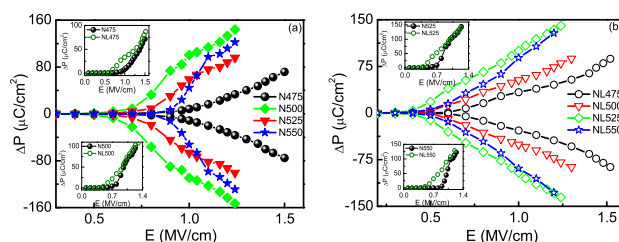


**Fig. 6** Switched polarization values  $\Delta P$  at different maximum electric fields of the BFO thin films (a) BFO/Ni, and (b) BFO/LSTO/Ni. For a given annealing temperature, the field dependent  $\Delta P$  is shown in inset.

## 4 Conclusions

BFO thin films were prepared on metallic Ni tapes by chemical solution deposition. The effects of annealing temperature as well as the introduction of a LSTO buffer layer have been investigated systematically. With increasing annealing temperature, the crystallite size, the dielectric constant and the leakage current density are increased, while the coercive field is decreased. On the other hand, the microstrain is increased with increasing annealing temperature. The remnant polarization increases initially and then decreases with increasing annealing temperature. At each given annealing temperature, some wrinkles caused by the large misfit in thermal expansion coefficient and lattice constant are observed in the BFO/Ni thin films, while it is not appeared in BFO/LSTO/Ni thin films.

As a result, the BFO/LSTO/Ni thin films exhibit better ferroelectric hysteresis loops and smaller coercive field due to the depression of wrinkles, reduction of microstrain as well as the improved leakage via the introduction of a LSTO buffer layer. These results will give a clear picture of the annealing temperature effects on the microstructure as well as the properties in CSD-derived BFO thin films on the flexible Ni tapes. In addition, it will provide an instructive route to prepare and optimize the properties of BFO thin films metallic tapes by the chemical solution deposition method.

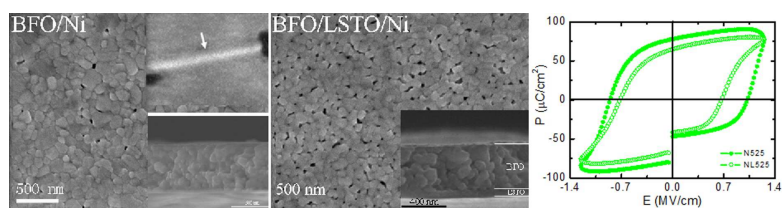
This work was supported by the National Science Foundation of China under Contract No.11204316.

## References

- 1 Y. E. Roginskaya, Y. Y. Tomashpol'skii, Y. N. Venevtsev, V. M. Petrov and G. S. Zhdanov, *Sov. Phys. JETP*, 1966, 23, 47-51.
- 2 G. Catalan and J. F. Scott. *Adv. Mater.*, 2009, 21, 2463-2485.
- 3 J. L. Wang, J. B. Neaton, H. Zheng, V. Nagarajan, S. B. Ogale, B. Liu, D. Viehland, V. Vaithyanathan, D. G. Schlom, U. V. Waghmare, N. A. Spaldin, K. M. Rabe, M. Wuttig and R. Ramesh, *Science*, 2003, 299, 1719-1722.
- 4 S. K. Singh, Y. K. Kim, H. Funakubo and H. Ishiwara, *Appl. Phys. Lett.*, 2006, 88, 162904.
- 5 S. Iakovlev, C.H. Solterbeck, M. Kuhnke and M. Es-Souni, *J. Appl. Phys.*, 2005, 97, 094901.
- 6 X. W. Tang, J. M. Dai, X. B. Zhu, J. C. Lin, Q. Chang, D. J. Wu, W. H. Song and Y. P. Sun *J. Am. Ceram. Soc.*, 2012,95, 538-544.
- 7 X. W. Tang, X. B. Zhu, J. M. Dai and Y.P. Sun, *Acta Materialia*, 2013, 61, 1739-1747.
- 8 J. T. Dawleya and P. G. Clem, *Appl. Phys. Lett.*, 2002, 81, 3028.
- 9 M. D. Losego, J. F. Ihlefeld and J. P. Maria, *Chem. Mater.*, 2008, 20, 303-307.
- 10 J. Weaver, Z. Yuan, J. Liu, G. Collins, C. L. Chen, J. C. Jiang, J. He, E. I. Meletis, R. Y. Guo, A. Bhalla, B. Lin, V. Giiurgiutiu and M. W. Cole, *Integr. Ferroelectr.*, 2008,100, 61-71.
- 11 D. I. Woodward, I. M. Reaney, G. Y. Yang, E. C. Dickey and C. A. Randall, *Appl. Phys. Lett.*, 2004, 84, 4650.
- 12 I. Bretos, T. Schneller, R. Waser, D. F. Hennings, S. Halder and F. Thomas, *J. Am. Ceram. Soc.*, 2010, 93, 3983-3985.
- 13 H. C. Lei, Y. P. Sun, X. B. Zhu, W. H. Song, J. Yang, and H. W. Gu, *IEEE Trans. Appl. Supercond.*, 2007, 17, 3819-3823
- 14 L. Yan, M. Zhuo, Z. Wang, J. Yao, N. Haberkorn, S. Zhang, L. Civale, J. Li, D. Viehland and Q. X. Jia, *Appl. Phys. Lett.*, 2012, 101, 012908.
- 15 J. Shin, A. Goyal, S. Jesse and L. Heatherly, *Appl. Phys. Express*, 2011, 4, 021501.
- 16 R. Y. Zheng, X. S. Gao, Z. H. Zhou and J. Wang, *J. Appl. Phys.*, 2007, 101, 054104.
- 17 Z. X. Cheng, H. Y. Zhao, Y. Du, H. Kimura, K. Ozawa and X. L. Wang. *Scr. Mater.*, 2011, 65, 249-252.
- 18 Y. J. Qi, Z. H. Chen, C. W. Huang, L. H. Wang, X. D. Han, J. L. Wang, P. Yang, T. Sritharan and L. Chen, *J. Appl. Phys.*, 2012, 111, 104117.
- 19 M. S. Kartavtseva, O. Y. Gorbenko, A. R. Kaul, A. R. Akbashev, T. V. Murzina, Fusil S, A. Barthlmy and F. Pailoux, *Surf. Coat. Technol.*, 2007, 201, 9149-9153.
- 20 S. K. Singh, K. Maruyama and H. Ishiwara, *Integr. Ferroelectr.*, 2008, 98, 83-89
- 21 H. Naganuma and S. Okamura, *J. Appl. Phys.*, 2007, 101, 09M103.
- 22 S. K. Singh, H. Ishiwara and K. Maruyama, *J. Appl. Phys.*, 2006, 100, 064102.
- 23 R. W. Schwartz, *Chem. Mater.*, 1997, 9, 2325-2340.
- 24 X. B. Zhu, S. B. Zhang, H. C. Lei, X. D. Zhu, G. Li, B. S. Wang, W. H. Song, Z. R. Yang, J. M. Dai, Y. P. Sun, D. Q. Shi and S. X. Do, *J. Am. Ceram. Soc.*, 2009, 92, 800-804.
- 25 F. Tyholdt, H. Fjellvag, A. E. Gunsøn and A. Olsen, *J. Appl. Phys.*, 2007,102, 074108
- 26 R. W. Schwartz, T. Schneller and R. Waser, *C.R. Chim.*, 2004, 7, 433-461.
- 27 Y. Wang, Y. H. Lin and C.W. Nan, *J. Appl. Phys.*, 2008, 104, 123912.
- 28 K. Zalamova, N. Roma', A. Pomar, S. Morlens, T. Puig, J. Gazquez, A. E. Carrillo, F. Sandiumenge, S. Ricart, N. Mestres and X. Obradors, *Chem. Mater.*, 2006, 18, 5897-5906
- 29 F. Xu, S. T. McKinstry, W. Ren, B. M. Xu, Z. L. Xie and K. J. Hemker, *J. Appl. Phys.*, 2001, 89, 1336.

- 
- 30 J. P. Cruz, E. Joanni, P. M. Vilarinho and A. L. Kholkin, *J. Appl. Phys.*, 2010, 108, 114106.
- 31 B. Nagaraj, S. Aggarwal, T. K. Song, T. Sawhney and R. Ramesh, *Phys. Rev. B*, 1999, 59, 16022-16027.
- 32 L. Jin, F. Li and S. J. Zhang, *J. Am. Ceram. Soc.*, 2014, 97, 1-27.
- 33 M. Dawber, K. M. Rabe and J. F. Scott, *Rev. Mod. Phys.*, 2005, 77, 1083-1130.
- 34 J. F. Scott and M. Dawber, *Appl. Phys. Lett.*, 2000, 76, 3801-3803.

## Table of Content



Introduction a  $\text{La}_{0.5}\text{Sr}_{0.5}\text{TiO}_3$  buffer layer is beneficial for microstructures and properties of  $\text{BiFeO}_3$  thin films on metallic tapes.